

## Biological and physical signatures in the tropical and subtropical Atlantic

S. R. Signorini,<sup>1,2</sup> R. G. Murtugudde,<sup>3,2</sup> C. R. McClain,<sup>4</sup>  
J. R. Christian,<sup>5,2</sup> J. Picaut,<sup>6,2</sup> and A. J. Busalacchi<sup>4</sup>

**Abstract.** The variability of sea surface chlorophyll concentration in the tropical and subtropical Atlantic during the first year of Sea-viewing Wide Field-of-view Sensor (SeaWiFS) imagery is examined. An Ocean General Circulation Model (OGCM) is used, along with TOPEX/Poseidon dynamic height observations and global gridded wind stress data sets, to explain the physical forcing of surface ocean color signals. Regions of high surface chlorophyll are strongly correlated with mesoscale and large-scale physical processes such as the strong upwelling off the west coast of Africa, the relatively high oceanic production within the Guinea Dome region, and the generation and propagation of large anticyclonic eddies along the coast of South America, north of the equator. The major river outflows (Amazon, Orinoco, and Congo) have strong signatures with plumes of apparently high Chl *a* in excess of 10 mg m<sup>-3</sup> near their deltas. The fall bloom in the eastern tropical Atlantic observed by the Coastal Zone Color Scanner (CZCS) was absent in 1997, whereas a bloom was observed in this region in July-September 1998, which was not observed by the CZCS. We attribute these apparent anomalies to the projection of the 1997-1998 El Niño event into the tropical Atlantic basin; these signals are correlated with sea surface temperature anomalies known to be associated with ENSO. The SeaWiFS images show that there are seasonal blooms within the hydrographic provinces of the Guinea and Angola domes. These hydrographic provinces are characterized by the dynamic uplift of the thermocline at the North Equatorial Current southern boundary (Guinea Dome) and the Benguela Current eastern boundary (Angola Dome). Within these domes, the Ekman pumping and transport are significant due to the strong trade winds at the surface. The Ekman drift plays a major role in the spreading of surface blooms. The spreading of the oceanic bloom at 12°N, 30°W, the Congo River plume, and the areal extent of the upwelling blooms off the coast of Africa, parallels the strength and extent of the Ekman surface drift. Upwelling, when broadly defined to include large scale vertical excursions of the thermocline, explains virtually all of the surface chlorophyll observations in excess of 0.5 mg m<sup>-3</sup>, except in the river plumes.

### 1. Introduction

The goal of this paper is twofold. First, we describe the observed spatial and temporal variability of surface

<sup>1</sup>SAIC-General Sciences Corporation, Beltsville, Maryland.

<sup>2</sup>Also at Laboratory for Hydrospheric Processes, NASA Goddard Space Flight Center, Greenbelt, Maryland.

<sup>3</sup>Earth System Science Interdisciplinary Center, University of Maryland, College Park.

<sup>4</sup>Laboratory for Hydrospheric Processes, NASA Goddard Space Flight Center, Greenbelt, Maryland.

<sup>5</sup>Universities Space Research Association, NASA Goddard Space Flight Center, Greenbelt, Maryland.

<sup>6</sup>L'Institut de Recherche pour le Développement (IRD-ORSTOM), France.

Copyright 1999 by the American Geophysical Union.

Paper number 1999JC900134.

0148-0227/99/1999JC900134\$09.00

Chl *a* observed by Sea-viewing Wide Field-of-view Sensor (SeaWiFS) during the 1997-1998 El Niño-La Niña event. Second, we correlate the observed spatial and temporal variability of Chl *a* in the tropical Atlantic with the upper ocean physical processes responsible for the surface manifestation of the biological processes in the euphotic zone. Therefore the following review of previous physical and biological studies in the tropical Atlantic is essential to set the stage for our analysis.

The first global distribution of the phytoplankton biomass near the ocean surface was provided by the Nimbus 7 Coastal Zone Color Scanner (CZCS). Although the CZCS mission was not designed to routinely collect global data [McClain *et al.*, 1993], the sampling in some areas and for some periods of time was adequate for resolving a variety of processes on spacescales and timescales ranging from mesoscale to global scale and from specific events to interannual variability. The most completely sampled basin was the North Atlantic

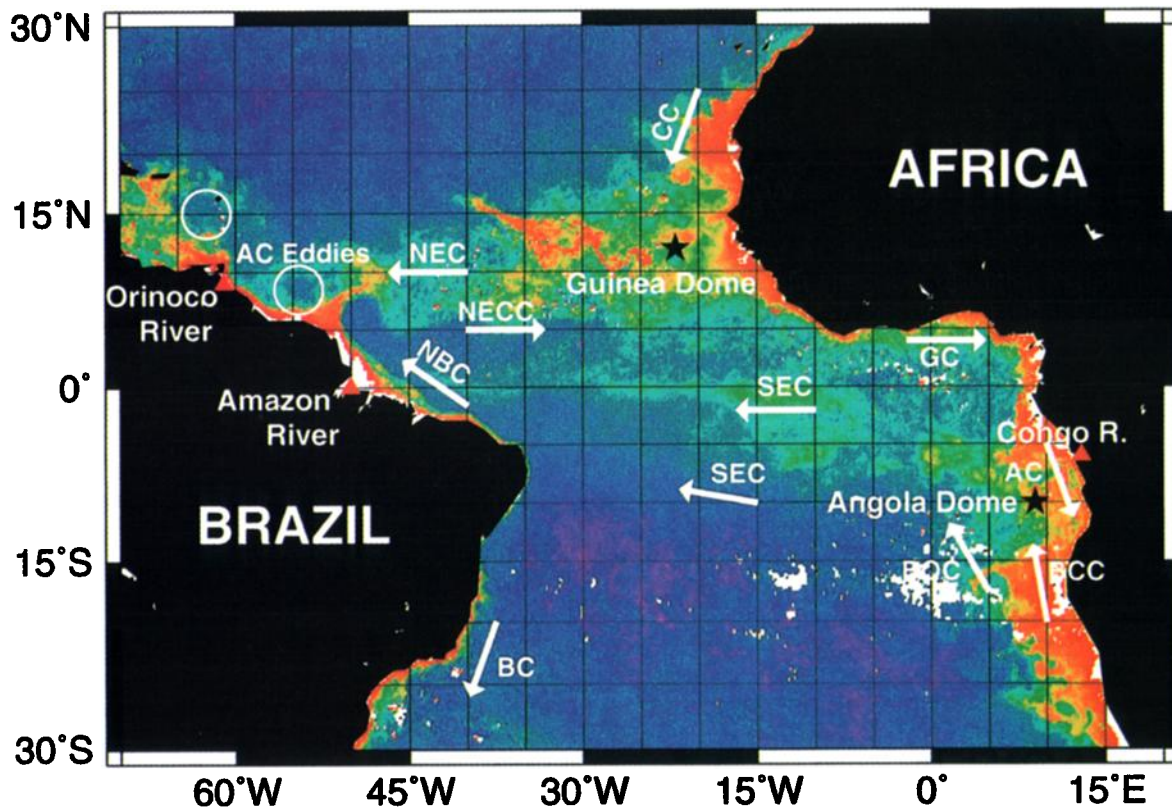


**Plate 1.** Schematic representation of tropical and subtropical Atlantic currents. A SeaWiFS Chl *a* image for the month of November 1997 is used to highlight the areas of high production. The system of currents represented here are the Canary Current (CC), North Equatorial Current (NEC), North Equatorial Counter Current (NECC), Guinea Current (GC), South Equatorial Current (SEC), Benguela Oceanic Current (BOC), Benguela Coastal Current (BCC), Angola Current (AC), North Brazil Current (NBC), and Brazil Current (BC). The black stars show the approximate location [Siedler *et al.*, 1992] of the Guinea and Angola Domes.

Ocean, where roughly 30% of the CZCS data were collected.

Studies using CZCS surface pigment data [McClain *et al.*, 1990; Platt *et al.*, 1991] showed that the spring bloom in the tropical Atlantic is sustained for 2 to 3 months in most locations. In addition, at a given latitude, the onset of the spring bloom varies by several months, and, in some cases, can be referred to as a fall bloom. Separate analyses of the mean pigment for the shelf and open ocean regions show that the phytoplankton of both regimes has spring and fall blooms of equal magnitude; the spring bloom being located at northern latitudes and the fall bloom in the equatorial region. These CZCS studies also reveal that annual primary production in the tropical Atlantic exceeds that of the entire North Atlantic bloom region. The estimated average annual production for the eastern tropical Atlantic (ETA) is  $2.3 \text{ Gt C yr}^{-1}$ , with a seasonal variability ranging from  $0.8$  to  $2.9 \text{ Gt C yr}^{-1}$  [Monger *et al.*, 1997].

Longhurst [1993] noted that the thermocline shoals dramatically in the ETA in response to seasonal intensification of the trade winds in the western tropical

Atlantic. He proposed that the dynamic uplift of the thermocline combined with mixing by local winds may be the principal mechanism controlling vertical nutrient fluxes and therefore phytoplankton blooms in the ETA. Monger *et al.* [1997] propose that in addition to seasonal change in the thermocline depth, one must also consider changes in the depth of the equatorial undercurrent to explain the prolonged bloom in the ETA (July through January).

Plate 1 shows a schematic representation of the tropical and subtropical Atlantic surface currents superimposed on a November 1997 monthly composite of SeaWiFS Chl *a*. The southern limb of the subtropical North Atlantic wind-driven gyre forms the clockwise system of currents consisting of the Canary Current (CC) off the northwest coast of Africa and the North Equatorial Current (NEC) extending across the basin between  $10^{\circ}\text{N}$  and  $15^{\circ}\text{N}$ . The northern limb of the subtropical South Atlantic wind-driven gyre forms the counterclockwise system of currents consisting of the Benguela Oceanic Current (BOC), the South Equatorial Current (SEC), and the Brazil Current (BC). The SEC branches to the northwest along the coast of Brazil

north of 5°S, forming the swift North Brazil Current (NBC). The NBC entrains fresh Amazon River water which is transported downstream to a latitude of about 5°N–10°N and carried several hundred kilometers offshore by the NBC retroflection. The discharge of the Amazon is carried by the NECC toward Africa between June and January of each year. From about February to May the countercurrent and the retroflection weaken or vanish, and Amazon water flows northwestward toward the Caribbean Sea [Muller-Karger *et al.*, 1988]. Note that the NBC retroflection has a distinctive signature in the Chl *a* image presented in Plate 1 marked by a transition zone between deep blue and light green colors where the thermocline is dynamically uplifted bringing nutrients to the euphotic zone.

Large-scale processes include the upwelling zone within the three principal hydrographic provinces, i.e., the Guinea and Angola domes, and the equatorial upwelling region in the Gulf of Guinea. The Guinea Dome is centered approximately at 12°N, 22°W. This shallow domelike thermocline feature is associated with counterclockwise flow fields composed of the eastward NECC and the westward NEC [Siedler *et al.*, 1992, Yamagata and Iizuka, 1995]. The primary source of the interannual upwelling signal for the North Atlantic is the region of NW Africa in the vicinity of the Guinea dome [McClain and Firestone, 1993]. The Angola Dome is located near 10°S, 9°E and does not exist during the boreal summer [Mazeika, 1967]. In these upwelling-favorable zones, there is an uplift of the thermocline and nitracline, which maintains an upward flux of nutrients within the euphotic zone. The intensity of the upwelling zones is governed by the variations in time and space of the trade winds, which have a strong annual component. As will be shown later in this paper, the surface Chl *a* fields from SeaWiFS exhibit spatial and temporal patterns that are coherent with sea surface height (SSH) and the thermocline depth, which are strongly coupled in the tropics [Rébert *et al.*, 1985].

In this paper, we use a year-long time series of SeaWiFS data (October 1997 to September 1998), combined with climatological CZCS data, to describe seasonal and interannual changes in the biological and physical characteristics of the tropical Atlantic euphotic zone. In addition, we identify the mechanisms responsible for the observed variability, and we analyze correlations among remote sensing and related data sets, including geophysical fields originating from an ocean general circulation model (OGCM).

## 2. Data Sources and Methods

Our analyses are based on data sets from diverse sources, including remote sensing data and results from ocean model simulations. Near-real time in situ data in the tropical Atlantic became available recently from the PIRATA array of moorings [Servain *et al.*, 1998], which is the Atlantic equivalent of TAO array in the

Pacific. However, the PIRATA program is still on its initial phase, and therefore the available data sets are limited in spatial and temporal coverage. Only water temperature down to 500 m and winds are currently available from six operational moorings which are providing data mostly from the beginning of 1998. In situ measurements of Chl *a*, nutrients, and primary production are extremely rare and usually taken for short periods of time at a few locations. Therefore we rely mostly on the Chl *a* data from SeaWiFS [McClain *et al.*, 1998].

The SeaWiFS data consist of Chl *a* from 8-day and monthly global standard mapped images (SMI) obtained from the NASA Goddard Distributed Active Archive Center (DAAC). These images have a resolution of about 9 km at the equator. We compare the SeaWiFS monthly composites with the CZCS 7.5-year monthly averages to highlight interannual differences. Although there are discrepancies between the CZCS and SeaWiFS algorithms for conversion to chlorophyll values, these discrepancies are primarily within the oligotrophic waters of the subtropical gyres and do not significantly affect comparisons of chlorophyll concentrations within the relatively high ( $\geq 0.2 \text{ mg m}^{-3}$ ) production regions of our study.

Monthly sea-surface height anomalies (SSHA) were obtained from TOPEX/Poseidon grids available at the NASA, GSFC Ocean PATHFINDER database. Sea-surface height (SSH), sea surface temperature (SST), depth of the thermocline, and current components were obtained from a decadal run for the tropical Atlantic, extending from 30°S to 30°N, using a reduced-gravity, primitive equation, sigma coordinate ocean GCM [Murtugudde and Busalacchi, 1998]. Yearly climatological nitrate and water temperature data were obtained from the Levitus world ocean atlas [Conkright *et al.*, 1994]. In addition, a simple analytical Ekman model was used to calculate the locally forced wind-driven component of the surface circulation and the Ekman pumping. The Ekman model uses daily winds obtained from the National Center for Environmental Prediction (NCEP) at NOAA.

## 3. Discussion

### 3.1. Equatorial Regimes

The equatorial regimes consist of the contributions from upwelling and two rivers discharging near the equator, the Congo and Amazon rivers. The Orinoco river discharge does not significantly influence the equatorial region since its plume is advected northwestward toward the Caribbean. Plate 2a and Plate 2b show a sequence of 12 monthly SeaWiFS composites for the period of October 1997 through September 1998. These pictures clearly show the major sources of Chl *a* (yellow to red plumes with concentrations  $\geq 1.0 \text{ mg m}^{-3}$ ) in the north and south tropical and subtropical Atlantic. The major rivers (Amazon, Orinoco, and Congo) have strong signatures with plumes of high Chl *a* in excess

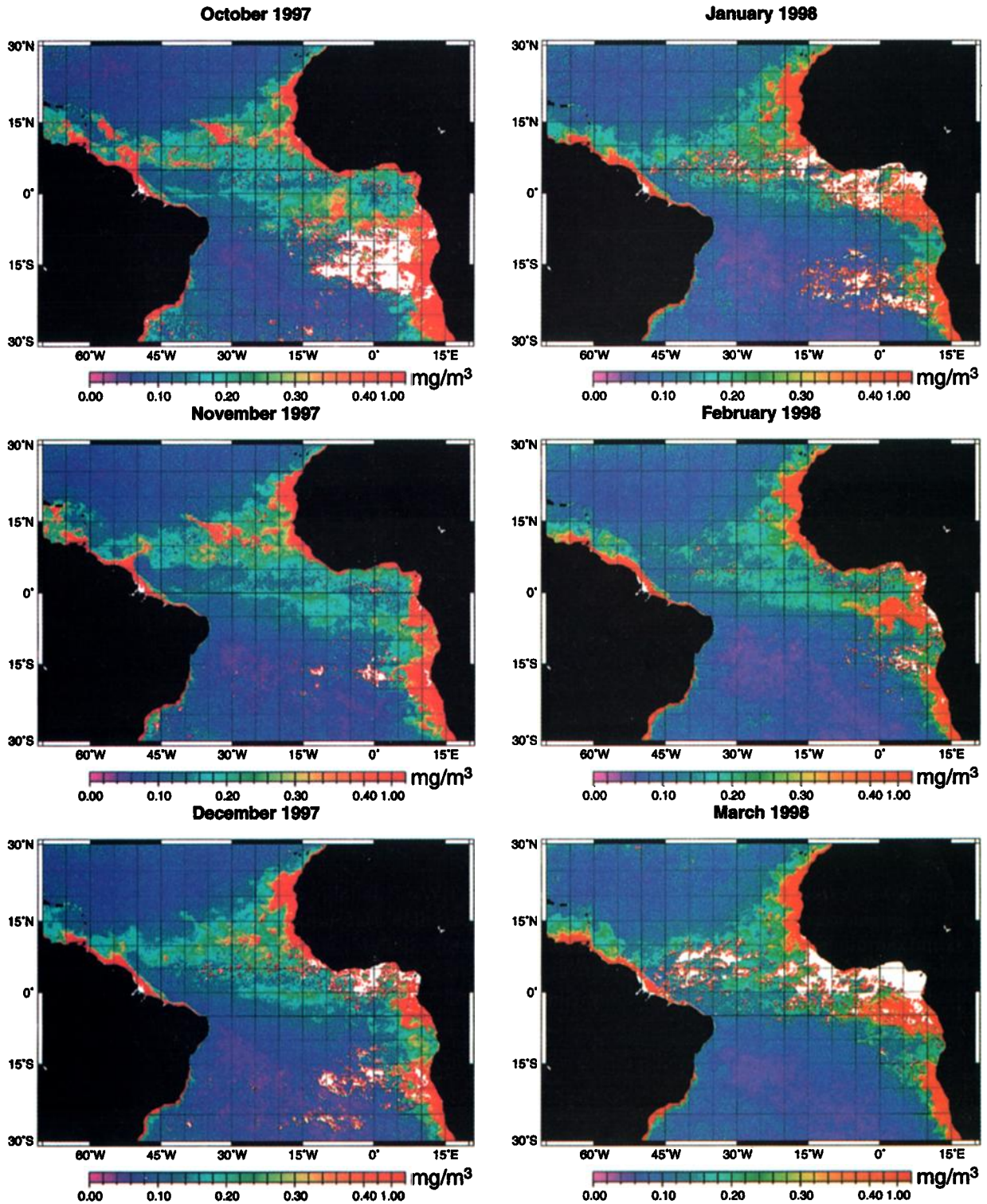


**Plate 2a.** Monthly mean Chl *a* for the tropical Atlantic observed by SeaWiFS (October 1997 to March 1998). Color palette increments are 0.02 from 0 to 0.4, then 0.5, 1.0, and  $\geq 1.0$ . White denotes missing values and values greater than 1.0 are red.

of  $10 \text{ mg m}^{-3}$  at their deltas. The global SeaWiFS Chl *a* algorithm is based on validation data collected largely in case I waters [O'Reilly *et al.*, 1998]. In a river plume the effects of absorption by dissolved organic substances (Gelbstoffe) and backscattering by flu-

vidial sediments make these estimates of Chl *a* concentration highly uncertain. The color signal is a useful indicator of the spread of the river plume, but it must be kept in mind that much of this signal may represent optically active substances other than Chl *a*. Estimates

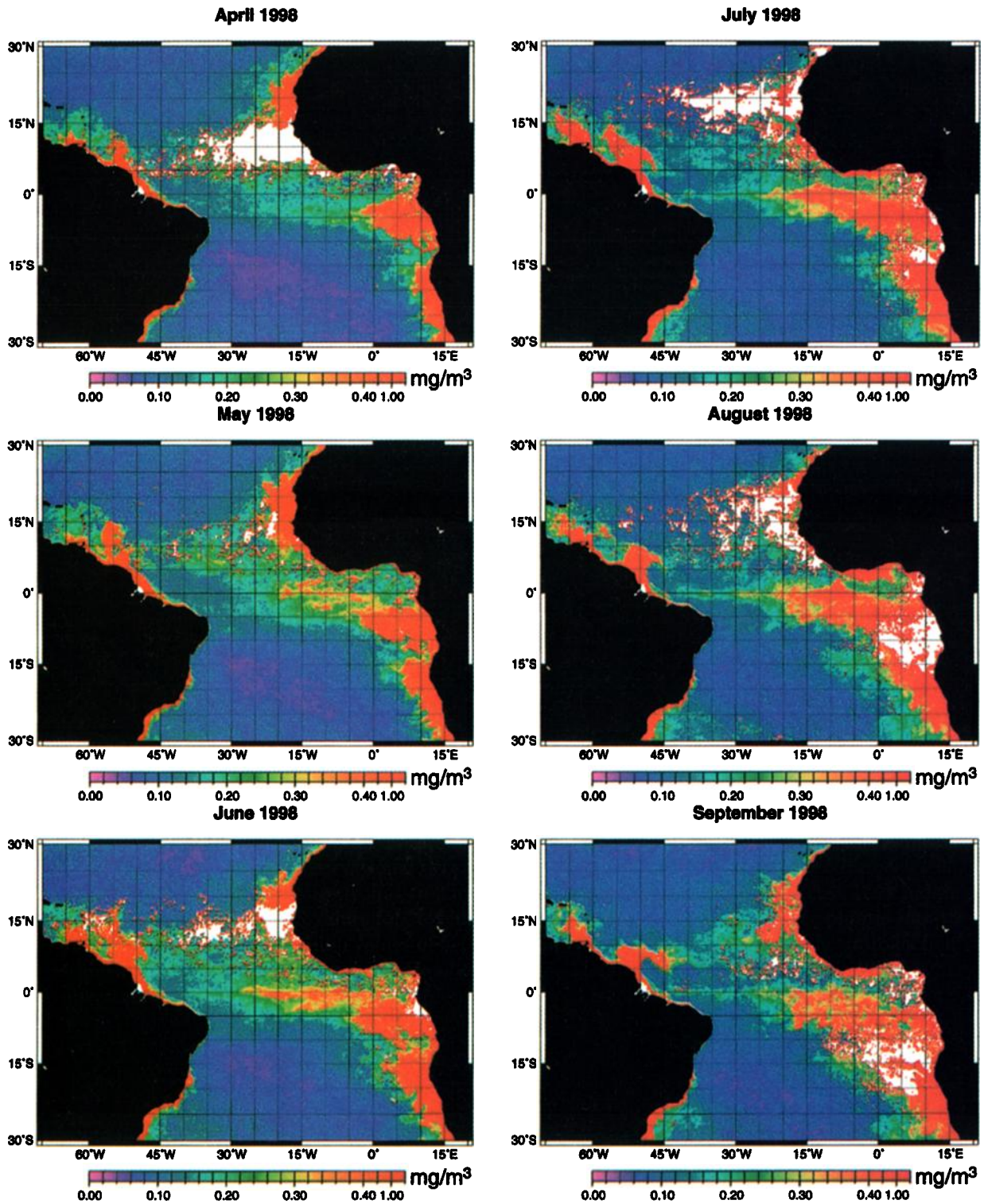


Plate 2b. Monthly mean Chl *a* for the tropical Atlantic observed by SeaWiFS (April - September 1998).

of Chl *a* concentrations in the Congo river plume are given by *Cadée* [1978] from a short observational period in November 1976. This estimates range from 1 to 2  $\text{mg m}^{-3}$ , which agree with the SeaWiFS values for November 1997. However, the actual maximum values of 5-10  $\text{mg m}^{-3}$  attained in later months (February-September 1998) are uncertain until in situ measurements become

available. The peak runoff from the Amazon ( $0^\circ\text{N}$ ,  $50^\circ\text{W}$ ) and Orinoco rivers [*Muller-Karger et al.*, 1989] occurs during April through August 1998 judging from the extensive penetration of their plumes into the open ocean, which further evidences the retroflection of the NBC. The Congo River plume ( $5^\circ\text{S}$ ,  $10^\circ\text{E}$ ) is very pronounced from January 1998 onward, and reaches a peak

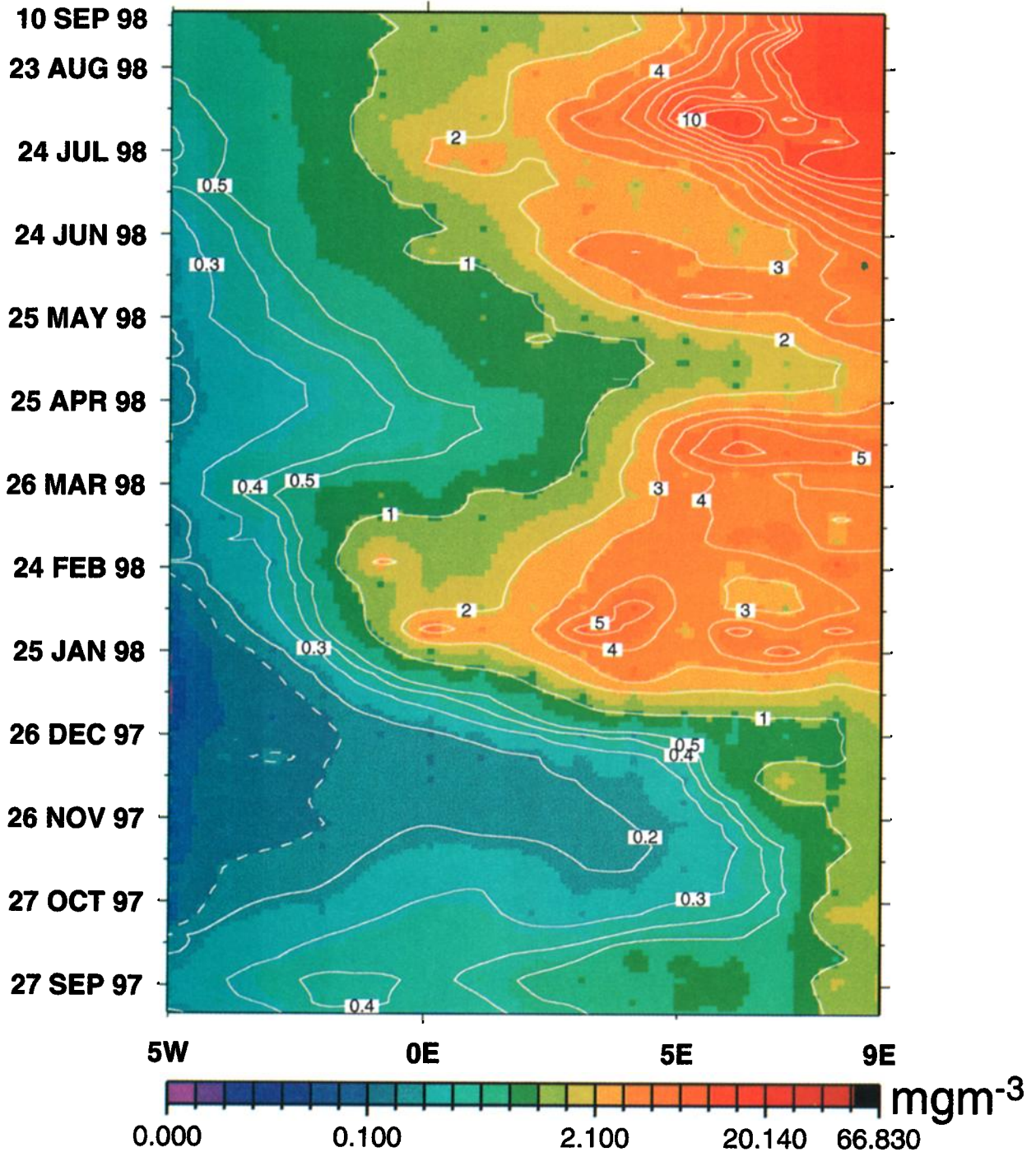


Plate 3. Longitude versus time plot of Chl *a* along 5°W-9°E centered at the Congo River plume (5°S).

during July-August 1998, in parallel with the coastal and equatorial upwelling. A zonal (5°W–9°E) phase plot of Chl *a* in the Congo River plume is presented in Plate 3. The fringe of the plume, defined here as the 1  $\text{mg m}^{-3}$  contour line, extends approximately 10° of latitude (1000 km) westward of its source at the river mouth.

In addition to the river plumes, there are other important sources of Chl *a* that are strictly related to wind-driven coastal upwelling. Note in Plate 2 the pres-

ence of large red patches off the northwest and southwest coasts of Africa throughout all months, and in the Gulf of Guinea starting in June and peaking in August. The surface manifestation of equatorial upwelling in the ETA began in May and grew in strength toward August 1998. This is an anomalous beginning of the upwelling season, which normally starts in the boreal summer [Monger *et al.*, 1997]. The intensification of equatorial upwelling is the result of the dynamic uplifting of the thermocline in the ETA in response to the in-

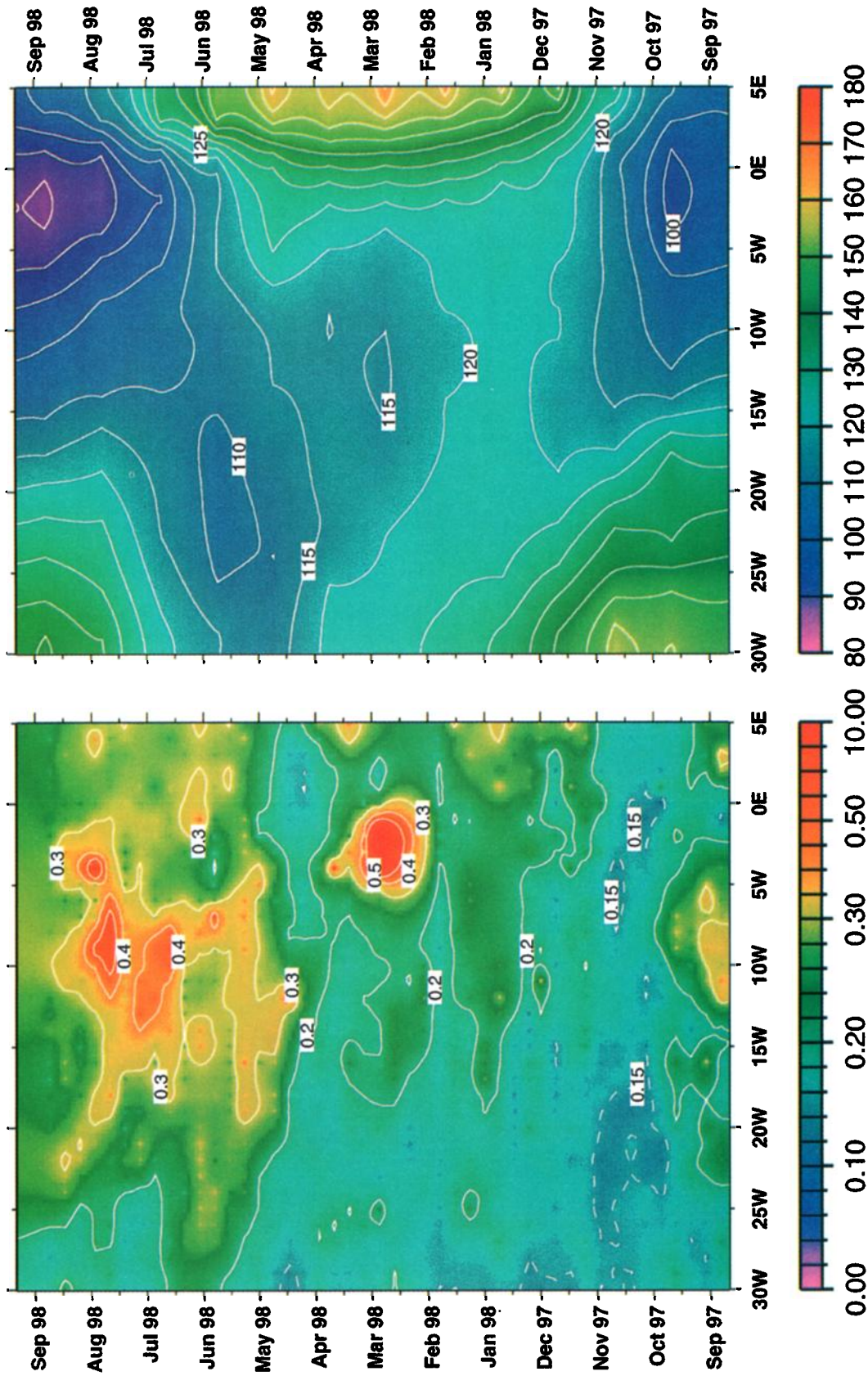


Plate 4. Longitude versus time plots of Chl *a* (in  $\text{mg m}^{-3}$ ) and depth (in meters) of the 20°C isotherm from the OGCM along 30°W-5°E and centered at the equator.

creasing easterly winds in the western tropical Atlantic [Moore et al., 1978; Busalacchi and Picaut, 1983]. Plate 4 shows zonal phase plots of the SeaWiFS Chl *a* and the depth of the 20°C isotherm along 30°W–5°E provided by the OGCM. During November 1997 to January 1998, the thermocline depth in the ETA was greater than 120 m deeper and Chl *a* values were  $\leq 0.2 \text{ mg m}^{-3}$  west of 4°E. Conversely, from the middle of February to the beginning of September, the thermocline depth decreased from 120 to 90 m in the ETA. This shallowing of the thermocline is accompanied by a correspondent bloom in the ETA with Chl *a* values  $\geq 0.3 \text{ mg m}^{-3}$ . This variability of the thermocline depth seems to be an unusually extreme seasonal pattern for 1997–1998. The seasonal deepening and shallowing of the thermocline has been reported in previous studies and attributed to the annual cycle of the surface wind field. Specifically, the seasonal intensification of the easterly winds in the western tropical Atlantic promotes the dynamic uplifting of the thermocline in the ETA, which in turn brings nutrients to the euphotic zone. Hastenrath and Merle [1987] show that, from around April to August–September the thermocline thins, intensifies, and its base rises, especially in the ETA; to the west there is some tendency for a deepening of the thermocline base and top. From after September to around April the thermocline thickens and weakens, its base deepens, again with particularly large effects in the ETA [Busalacchi and Picaut, 1983].

### 3.2. Guinea and Angola Dome Regimes

The SeaWiFS images in Plates 2a and 2b show seasonal blooms within the hydrographic provinces of the Guinea and Angola domes. These hydrographic provinces are characterized by the dynamic uplift of the thermocline at the NEC-NECC boundary (Guinea Dome) and the Benguela Current eastern boundary (Angola Dome). This dynamic uplift of the thermocline follows the nearly geostrophic adjustment in response to strong wind curl forcing. Within these domes, the Ekman pumping and transport are significant due to the strong trade winds at the surface and their spatial variability (curl of the wind). In addition, the uplifting of the deeper thermal structure is caused by the north and south equatorial undercurrents [Voituriez, 1981]. To investigate the physical-biological interactions within the dome regimes, we calculate the Ekman vertical velocity ( $w_e$ ) and transport ( $\vec{T}_e$ ) fields using NCEP diagnostic daily winds and the following equations:

$$\vec{T}_e = \vec{k} \times \left( \frac{\vec{\tau}}{\rho f} \right) \quad (1)$$

$$w_e = \nabla \cdot \vec{T}_e = \vec{k} \nabla \times \left( \frac{\vec{\tau}}{\rho f} \right) \quad (2)$$

where  $\vec{\tau}$  is the wind stress (calculated from the wind velocity components),  $\rho$  is the water density,  $f(\phi)$  is the Coriolis parameter,  $\phi$  is the latitude, and  $\vec{k}$  is the unit vector pointing upward. Note that since  $f$  vanishes

at the equator, a minimum latitude at which (1) and (2) are finite must be adopted. We limit our domain to the latitude boundaries of 5°N–30°N and 5°S–30°S.

In addition to the Ekman transport and vertical velocity, another useful quantity to analyze the effects of advection on the Chl *a* distribution is the Ekman surface flow. SeaWiFS sees the surface manifestation of the blooms so that an assessment of the surface currents is important in correlating the observed patterns of Chl *a* with advective processes. The wind-driven Ekman drift [Neumann and Pierson, 1966] velocity at the surface ( $V_o$ ) is given by

$$V_o = \frac{\tau}{\sqrt{2A\rho\omega\sin\phi}} \quad (3)$$

where  $A$  is the eddy viscosity coefficient,  $\omega$  is the Earth's rotation frequency, and  $\phi$  is the latitude. The direction of  $V_o$  is 45° to the right of  $\vec{\tau}$  in the northern hemisphere and 45° to the left of  $\vec{\tau}$  in the southern hemisphere. The value of  $A$  used is  $28 \text{ m}^{-1} \text{ kg s}^{-1}$  and the Ekman depth,  $D = \pi(2A/f\rho)^{0.5}$ , ranges from 200 m at 5°N, 5°S to 87 m at 30°N, 30°S.

Plate 5 shows the Ekman pumping velocity field (in  $\text{m d}^{-1}$ ) with superimposed vectors of Ekman transport (in  $\text{m}^3 \text{ s}^{-1} \text{ m}^{-1}$ ) for the months of November 1997 and June 1998. These two months highlight the Guinea dome bloom (November 1997) and the onset of upwelling in the ETA (June 1998). Plate 6 shows the SeaWiFS monthly Chl *a* with OGCM SSH (cm) and vectors of surface Ekman drift ( $\text{m s}^{-1}$ ) superimposed. We chose to display the OGCM SSH field, instead of SSHA from TOPEX/Poseidon, because it streamlines the path of the geostrophic currents allowing a comparison with the surface Ekman drift. In areas of high SSH gradient the geostrophic component is dominant, whereas in areas of weak SSH gradient the dominant component is the Ekman drift (as in the Guinea Dome region). Note in Plate 5 that the Ekman transport is directed from the equatorial region and upwelling regions off the coast of Africa toward the center of the subtropical gyres. Intense Ekman pumping ( $0.3\text{--}0.5 \text{ m d}^{-1}$ ), denoted by the yellow-red regions, is present every month in the equatorial and upwelling regions. The combination of the horizontal and vertical Ekman transports are key mechanisms for the supply of nutrients into the euphotic zone. Williams and Follows [1998] showed that there is a large Ekman supply of nitrate at the tropical/subtropical boundary in the North Atlantic, where the easterly winds drive a poleward flux of tropical waters with high nutrients. However, we postulate that in order to maintain a steady supply of nutrients in the euphotic zone, a deeper mechanism, which taps the deep pool of nutrients in the ocean, must exist in combination with the Ekman processes. This mechanism is the doming of the thermocline due to strong horizontal shear along the boundaries of the major ocean currents. Specifically, Plate 6 shows a significant bloom centered at 12°N, 32°W inside the Guinea dome during Novem-

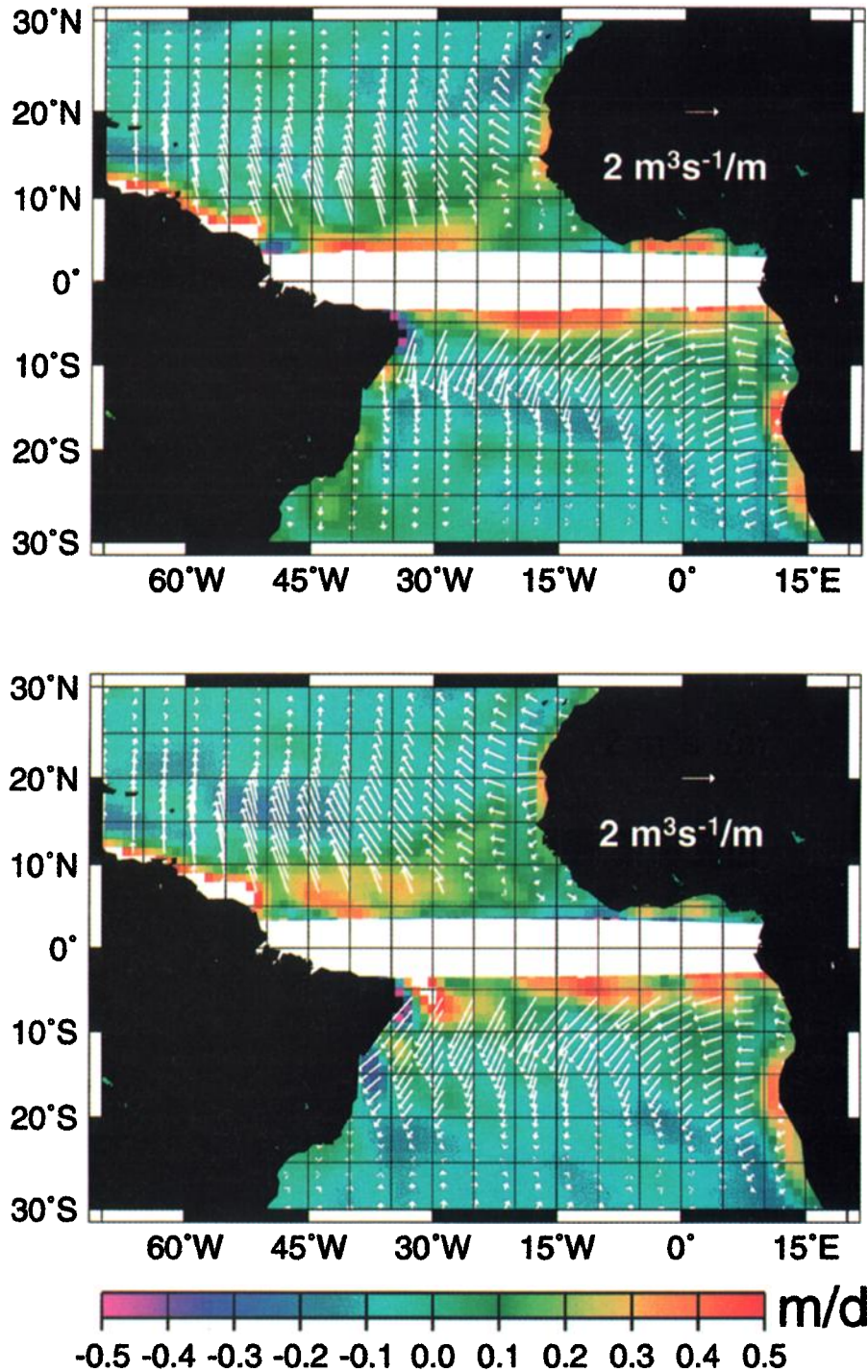


**Plate 5.** Monthly Ekman pumping ( $\text{m d}^{-1}$ ) and Ekman transport ( $\text{m}^3 \text{s}^{-1} \text{m}^{-1}$ ) for November 1997 and June 1998 in the tropical Atlantic.

ber 1997. In November the NECC was very strong and close to the NEC flowing in the opposite direction. This can be seen in the SSH fields from the OGCM, which show a long and narrow SSH minimum that extends from 20°N near the coast of Africa to the coast of South America at 10°N. This minimum in SSH corresponds to the boundary between these two opposing currents and is manifested as a result of the combined effect of the two currents uplifting the thermocline. Also note

that the bloom at 12°N, 32°W is enclosed by a contour of minimum SSH during November. This minimum in SSH corresponds to an anomalous thermocline depth of less than 80 m. The nitracline closely follows the rising thermocline and higher nitrate concentrations become available within the euphotic zone causing the observed bloom. The shape of the bloom is elongated along a SE-NW direction, in close agreement with the direction of the surface Ekman drift. Also note that the

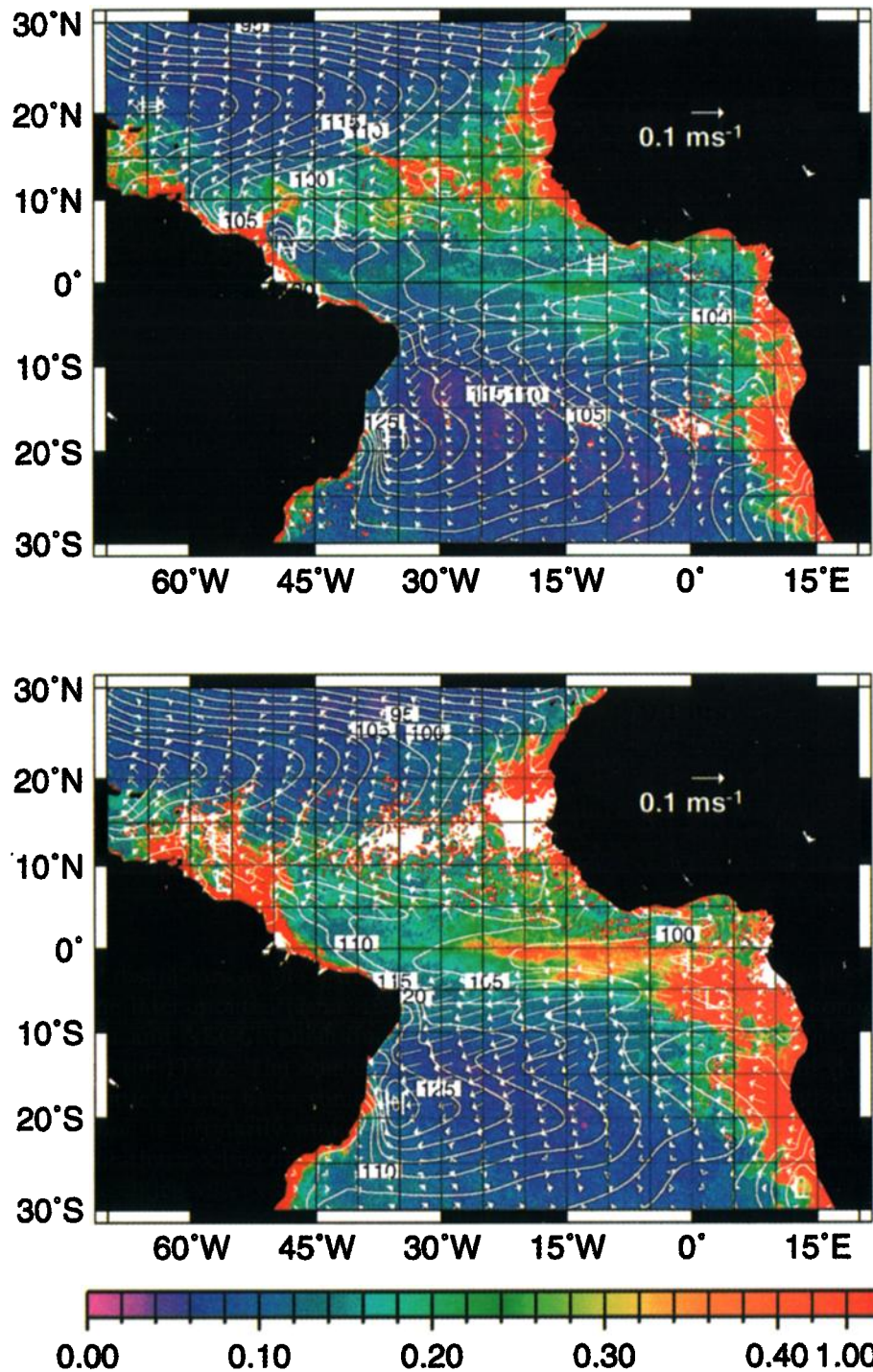


**Plate 6.** SeaWiFS monthly Chl *a* ( $\text{mg m}^{-3}$ ), OGCM SSH (cm), and Ekman surface flow ( $\text{m s}^{-1}$ ) for November 1997 and June 1998 in the tropical Atlantic.

surface bloom weakens and disappears as the SSH minimum broadens towards the later months (June 1998) when the NBC retroflection and NECC vanish due to the southward migration of the ITCZ. The scenario in the southern tropical Atlantic (Plate 6) is somewhat different. The Angola dome is primarily maintained by the dynamic uplift of the thermocline driven by the Benguela-SEC system. The width and extension of the

dome, which is also manifested in the OGCM SSH fields, is defined by the intensity and horizontal shear of the southeasterly trades. This can be seen in the coherent pattern between the width of the dome, defined by the tongue of SSH distribution, and the meridional shear in the surface Ekman drift. The spreading of surface blooms in the domes is probably a combination of surface Ekman drift and Rossby wave propagation [Hof-

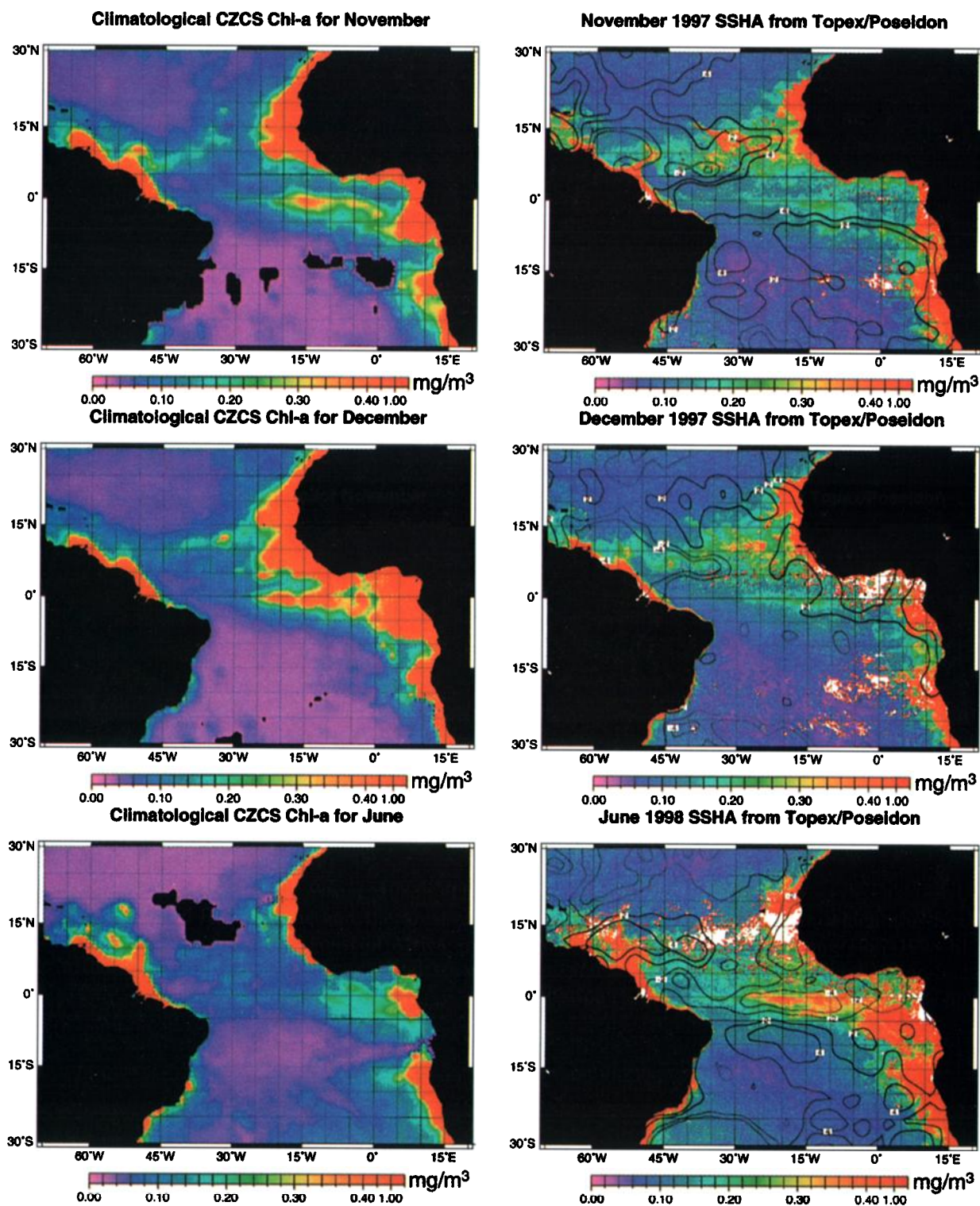


**Plate 7.** Comparison between SeaWiFS Chl *a* for November, December 1997, and June 1998, with equivalent CZCS monthly composites. The SeaWiFS plates have the TOPEX/Poseidon SSHA (cm) fields superimposed.

*mann et al.*, 1981; *Busalacchi and Picaut*, 1983]. The spreading of the Congo River plume and the areal extent of the upwelling blooms off the coast of Africa are coherent with the strength and extent of the Ekman surface drift.

### 3.3. Interannual Variability

The anomalous period under which the SeaWiFS data were collected, i.e., the strong 1997-1998 El-Niño event, and the effects that the Pacific El Niño-Southern Oscillation (ENSO) variability may have on the physical

and biological processes in the tropical Atlantic, inspire a closer look at the interannual variability captured by the available data sets. *Enfield and Mayer* [1997] show that the tropical Atlantic SST variability is correlated with Pacific ENSO variability in several regions. The major region affected is the North Tropical Atlantic area of NE trades west of 40°W along 10°N–20°S and extending into the Caribbean. There, about 50–80% of the anomalous SST variability is associated with the Pacific ENSO, with tropical Atlantic warmings occurring usually 4–5 months after the mature phases of the Pacific warm events. *Enfield and Mayer* [1997] show, from an analysis of local surface fields derived from COADS data, that the ENSO-related tropical Atlantic warmings occur as a result of reductions in the surface NE trade wind speeds, which in turn reduce latent and sensible heat losses over the region in question, as well as cooling due to entrainment.

We address the interannual variability of equatorial blooms by resorting to the longest temporal coverage of surface Chl *a* available, e.g., the CZCS data set. The 7.5 years of CZCS data provide monthly composites that are extremely helpful in determining departures from the mean seasonal cycle of surface Chl *a* in the tropical Atlantic. However, it should be noted that most of the CZCS data coverage occurred during 1978–1979, thus representing non-El Niño average condition rather than a 7.5-year climatological average. Plate 7 combines CZCS monthly climatologies for November, December, and June, and monthly SeaWiFS composites for November–December 1997 and June 1998. The monthly SeaWiFS composites also have the TOPEX/Poseidon SSHA contours (in cm) superimposed on the color images of Chl *a*. We converted the pigment concentrations from CZCS to Chl *a* concentrations using the conversion coefficient of 0.76 suggested by *Balch et al.* [1992].

A comparison between the CZCS pigment concentration and SeaWiFS Chl *a* reveals a significant difference in the timing and intensity of the tropical Atlantic blooms. The composite CZCS image for December shows a significant seasonal bloom ( $\geq 1.0 \text{ mg m}^{-3}$ ) along the equator east of 30°W, associated with the secondary upwelling season in the ETA [*Busalacchi and Picaut*, 1983], while in December 1997, the Chl *a* concentrations from SeaWiFS at the same location are  $\leq 0.26 \text{ mg m}^{-3}$ . Conversely, the seasonal climatological pigment concentration for June at the same equatorial region ranges from 0.15 to 0.3  $\text{mg m}^{-3}$ , while the SeaWiFS Chl *a* ranges from 0.3 to 0.5  $\text{mg m}^{-3}$ . This significant contrast in concentrations highlights the anomalous behavior of the upper ocean ecosystem processes in the Tropical Atlantic coincident with the 1997–1998 El Niño. Also note that the areal extension of high pigment concentrations off NW Africa for the fall (November–December) is much larger than the Chl *a* concentrations from SeaWiFS during November–December 1997. This anomalous decrease in Chl *a* concentrations results from

a reduction in the wind intensity which weakens the upwelling process off NW Africa and deepens the thermocline in the ETA [*Hastenrath and Merle*, 1987]. Thus the Chl *a* concentrations observed by SeaWiFS are consistent with the anomalous physical forcing during the 1997–1998 El Niño. The superimposed TOPEX/Poseidon SSH anomalies on the SeaWiFS images confirm the above scenario. These SSH anomalies are relative to a 1993 mean sea surface height network of ERS-1 and TOPEX/Poseidon georeferenced groundtracks. During November–December 1997, the SSH was 2 to 8 cm above normal in the ETA, indicating a deepening of the thermocline. Conversely, during June 1998, the SSH was 2 to 4 cm below normal in the ETA, an indication that the thermocline was shallower than normal for that time of the year. The SST anomaly fields for November 1997 and June 1998 (Plate 8), obtained from subtracting the COADS SST climatology from the *Reynolds and Smith* [1994] monthly SST fields, also indicate an anomalous interannual scenario. The SST within the NE trades zone (west of 15°W and north of 5°N) was 0.5°C to 1°C warmer than normal from November 1997 through June 1998. These SST anomalies are consistent with the anomalous nature of the 1997–1998 Chl *a* surface distributions. Note that the SST in the upwelling zone off of Angola is more than 2°C warmer than normal from November 1997 through June 1998. This warming trend extends northward to the ETA during June 1998.

### 3.4. Mean Fields

To better illustrate the correlations between the euphotic zone biological processes and the physical fields, we provide an analysis of the 12-month Chl *a* mean distribution obtained from the average of all SeaWiFS monthly composites (October 1997 to September 1998). Plate 9 shows the 12-month Chl *a* images with superimposed contours of Levitus yearly-averaged water temperature at 100 m (T100), the Levitus yearly-averaged nitrate concentration at 100 m, and the OGCM 12-month mean T100, D20 (depth of the 20-m isotherm), SST, and SSH.

All superimposed fields are coherent with the Chl *a* 12-month mean distribution. The "blue water" (Chl *a*  $\leq 0.1$ ) lies in the center of the subtropical gyres and correlates with warmer SST and T100, a deeper thermocline (D20  $\geq 300$  m) and high SSH ( $\geq 120$  cm), and 100-m nitrate concentrations  $\leq 2 \mu\text{M}$ . The high Chl *a* concentration within the Congo River plume overlays the tongue of  $\text{NO}_3 \geq 20 \mu\text{M}$ . The river water contains 5–8  $\mu\text{M}$  nitrate, and Redfield equivalent or greater phosphate and silicate concentrations [*van Bennekom et al.*, 1978]. If the river plume is defined as the 20 psu contour, the potential new production from fluvial nutrients is equivalent to 2–3  $\text{mg m}^{-3}$  of chlorophyll, assuming 1 mg of Chl *a* per mole of nitrogen.

The upwelling regions off NW and SW Africa, and the eastern equatorial Atlantic, are characterized by 100-m

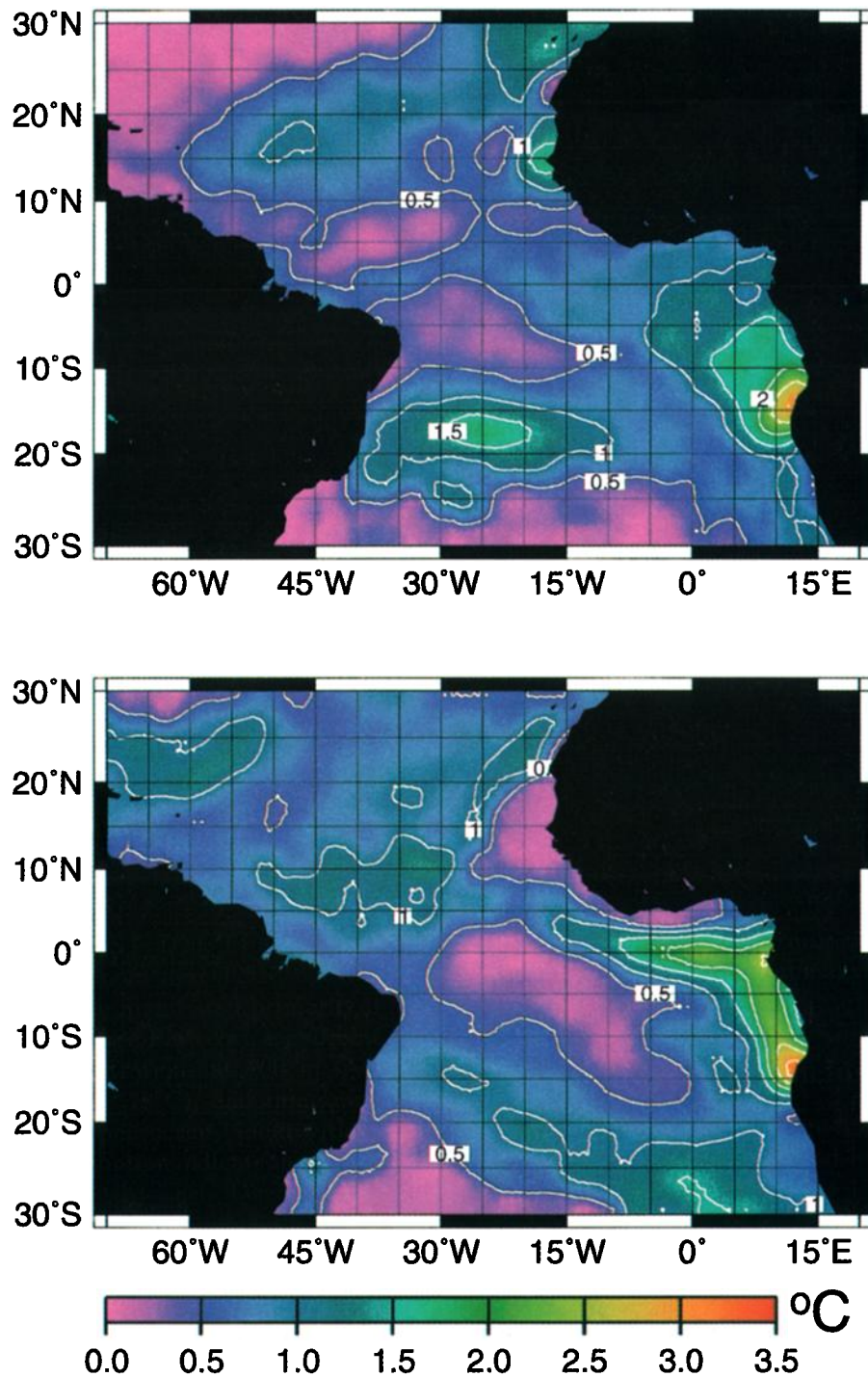


Plate 8. Monthly SSTA for November 1997 and June 1998.

$\text{NO}_3 \geq 12 \mu\text{M}$ , minimum SST, D20, T100, and SSH values. The open ocean bloom near  $12^\circ\text{N}$ ,  $32^\circ\text{W}$  in the Guinea dome, which was manifested primarily during October–December 1997 (see Plate 2a), is coherent with maximum nitrate concentrations at 100 m ( $\text{NO}_3 \geq 20 \mu\text{M}$ ), minimum T100 ( $T \leq 18^\circ\text{C}$ ), and minimum SSH. The correlation of this open ocean bloom with the climatological nitrate distribution indicate that the Guinea dome feature is a persistent one. Longer time series

of SeaWiFS data will be required to extend and confirm the seasonal and interannual variability of all these blooms.

#### 4. Summary and Conclusions

We describe the observed spatial and temporal variability of surface Chl *a* observed by SeaWiFS during a period which corresponds to the 1997–1998 El Niño–La

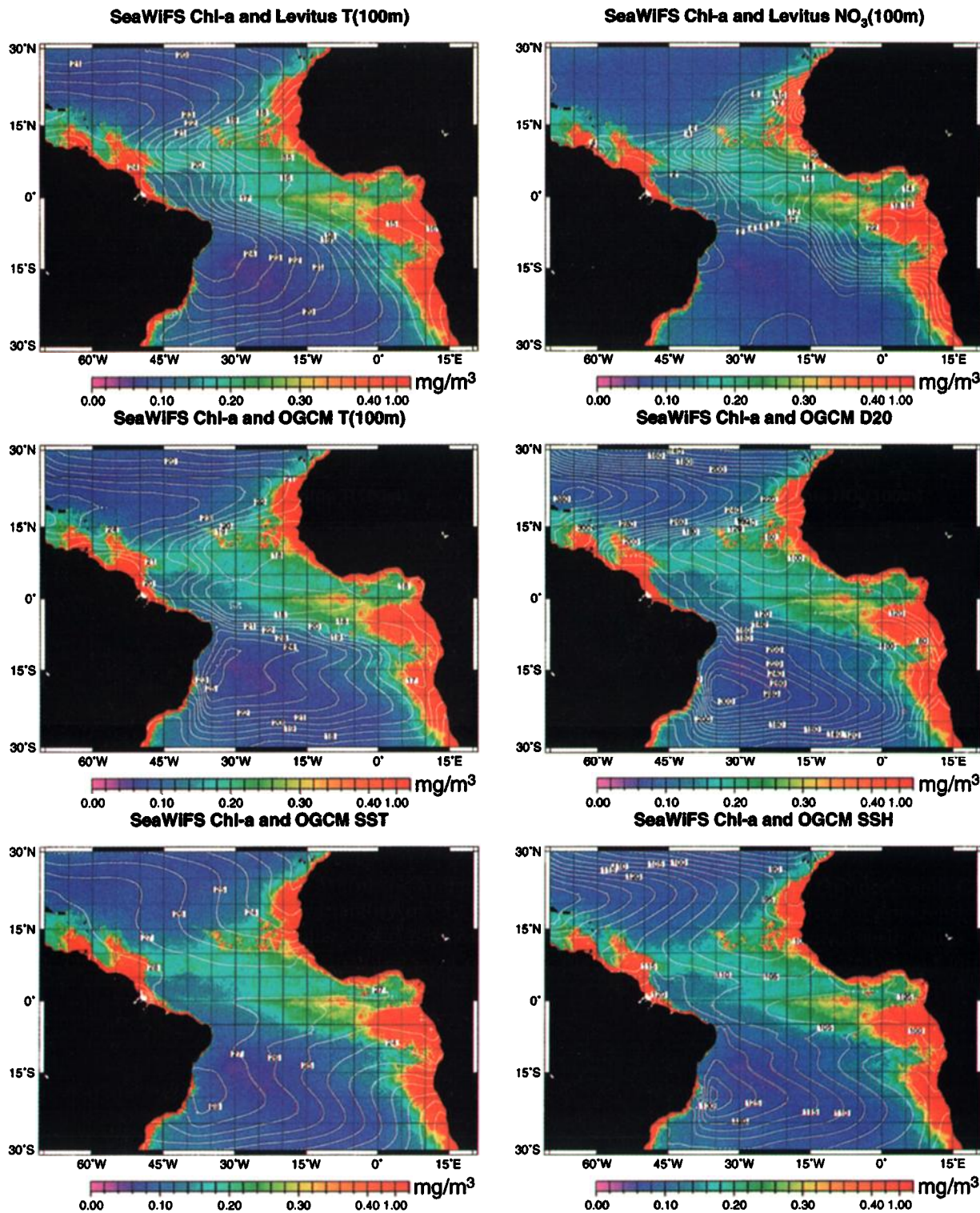


**Plate 9.** Twelve-month mean Chl *a* for the tropical Atlantic observed by SeaWiFS with Levitus T100m and NO<sub>3</sub> yearly climatology, and 12-month mean OGCM SSH, T100m, SST, and D20°C superimposed.

Niña event of the tropical Pacific. We also correlate the observed spatial and temporal variability of Chl *a* in the tropical Atlantic with the upper ocean physical processes responsible for the surface manifestation of the coupled biological processes in the euphotic zone.

The major rivers (Amazon, Orinoco, and Congo) have strong signatures with plumes of apparently high Chl *a* in excess of 10 mg m<sup>-3</sup> near their deltas. The peak runoff for the Amazon (0°N, 50°W) and Orinoco rivers occurs during April through August 1998. The

Congo River plume (5°S, 10°E) is very pronounced from January 1998 onward but reaches a peak during July–August 1998.

In addition to the river plumes, there are other important sources of Chl *a* that are related to wind-driven coastal upwelling. Large patches of high Chl *a* are observed off the northwest and southwest coasts of Africa throughout all months and along the north coast of the Gulf of Guinea starting in June and peaking in August. The equatorial upwelling in the ETA did not manifest itself in the surface Chl *a* until May and grew in strength toward August 1998. This intensification of equatorial upwelling is a response to the dynamic uplifting of the thermocline in the ETA associated with the increasing trades in the western tropical Atlantic. This dynamic uplifting mechanism, combined with the supply of nitrate from Ekman pumping transport from the equatorial upwelling regions to the subtropical gyres, constitute an important mechanism for the maintenance of relatively high levels of chlorophyll in the ETA.

The composite CZCS images for November and December show a significant seasonal bloom ( $\geq 1.0$  mg m<sup>-3</sup>) along the equator east of 30°W, while in November and December, 1997, the Chl *a* concentrations from SeaWiFS at the same location are  $\leq 0.26$  mg m<sup>-3</sup>. Conversely, the seasonal CZCS Chl *a* concentration for June at the same equatorial region ranges from 0.15 to 0.3 mg m<sup>-3</sup>, while the SeaWiFS Chl *a* concentrations for June 1998 range from 0.3 to 0.5 mg m<sup>-3</sup>. This significant contrast in concentration highlights the anomalous behavior of the upper ocean ecosystem processes resulting from wind changes associated with the influence of the 1997–1998 El Niño in the tropical Atlantic Ocean.

The year-long SeaWiFS data, combined with CZCS composite images, provided further insight to the upper ocean coupled biophysical processes. The continuous enlargement of the SeaWiFS data archive will provide longer time series that will allow us to extend and confirm the seasonal and interannual variability of tropical Atlantic blooms. In addition, we look forward to continue this research using a fully coupled ecosystem model that will allow a more in-depth analysis of the biophysical interactions.

**Acknowledgments.** We acknowledge the following grants that helped support this work. NASA RTOP 622-51-30 (Ocean Biogeochemistry), NASA RTOP 622-32-52-21 (TRMM) and 621-55-24 (TOPEX Extended Mission), and NASA RTOP 665-55-04-02 (TOPEX Extended Mission) and 622-48-02-00.

## References

- Balch, W., R. Evans, J. Brown, G. Feldman, C. McClain, and W. Esaias, The remote sensing of ocean productivity: Use of a new data compilation to test satellite algorithms, *J. Geophys. Res.*, **97**, 2279–2293, 1992.
- Busalacchi, A. J., and J. Picaut, Seasonal variability from a model of the tropical Atlantic Ocean, *J. Phys. Oceanogr.*, **13**, 1564–1588, 1983.
- Cadée, G. C., Primary production and chlorophyll in the Zaire River, estuary and plume, *Netherlands J. Sea Res.*, **12**, 369–381, 1978.
- Conkright, M., S. Levitus, and T. Boyer, *NOAA Atlas NES-DIS 1, World Ocean Atlas 1994*, Vol. 2, *Temperature*, 150 pp., U.S. Dep. of Comm., Washington, D. C., 1994.
- Enfield, D. B., and D. A. Mayer, Tropical Atlantic sea surface temperature variability and its relation to El Niño–Southern Oscillation, *J. Geophys. Res.*, **102**, 929–945, 1997.
- Hastenrath, S., and J. Merle, Annual cycle of subsurface thermal structure in the tropical Atlantic ocean, *J. Phys. Oceanogr.*, **17**, 1518–1538, 1987.
- Hofmann, E. E., A. J. Busalacchi, and J. J. O'Brien, Wind generation of the Costa Rica dome, *Science*, **214**, 552–554, 1981.
- Longhurst, A., Seasonal cooling and blooming in tropical oceans, *Deep Sea Res., Part I*, **40**, 2145–2165, 1993.
- Mazeika, P. A., Thermal domes in the eastern tropical Atlantic Ocean, *Limnol. Oceanogr.*, **12**, 537–539, 1967.
- McClain, C. R., W. E. Esaias, G. C. Feldman, J. Elrod, D. Endres, J. Firestone, M. Darzi, R. Evans, and J. Brown, Physical and biological processes in the North Atlantic during the First GARP Global Experiment, *J. Geophys. Res.*, **95**, 18,027–18,048, 1990.
- McClain, C. R., and J. Firestone, An investigation of Ekman upwelling in the North Atlantic, *J. Geophys. Res.*, **98**, 12,327–12,339, 1993.
- McClain, C. R., G. Feldman, and W. Esaias, Oceanic biological productivity, in *Atlas of Satellite Observations Related to Global Change*, edited by R. J. Gurney, J. L. Foster, and C. L. Parkinson, pp. 251–263, Cambridge Univ. Press, New York, 1993.
- McClain, C. R., M. L. Cleave, G. C. Feldman, W. W. Gregg, S. B. Hooker, and N. Kuring, Science quality SeaWiFS data for global biosphere research, *Sea Technol.*, 10–16, Sept. 1998.
- Monger, B., C. R. McClain, and R. G. Murtugudde, Seasonal phytoplankton dynamics in the eastern tropical Atlantic, *J. Geophys. Res.*, **102**, 12,389–12,411, 1997.
- Moore, D. W., P. Hisard, J. P. McCreary, J. Merle, J. J. O'Brien, J. Picaut, J.-M. Verstraete, and C. Wunsch, Equatorial adjustment in the eastern Atlantic, *Geophys. Res. Lett.*, **5**, 637–640, 1978.
- Muller-Karger, F. E., C. R. McClain, and P. L. Richardson, The dispersal of the Amazon's water, *Nature*, **333**, 56–59, 1988.
- Muller-Karger, F. E., C. R. McClain, T. R. Fischer, W. E. Esaias, and R. Varela, Pigment distribution in the Caribbean Sea: Observations from space, *Prog. Oceanogr.*, **23**, 23–64, 1989.
- Murtugudde, R. G., and A. J. Busalacchi, Salinity effects in a tropical ocean model, *J. Geophys. Res.*, **103**, 3283–3300, 1998.
- Neumann, G., and W. J. Pierson Jr., *Principles of Physical Oceanography*, Prentice-Hall, Englewood Cliffs, N. J., 1966.
- O'Reilly, J. E., S. Maritorena, B. G. Mitchell, D. A. Siegel, K. L. Carder, S. A. Garver, M. Kahru, and C. McClain, Ocean color chlorophyll algorithms for SeaWiFS, *J. Geophys. Res.*, **103**, 24,937–24,953, 1998.
- Platt, T., C. Caverhill, and S. Sathyendranath, Basin-scale estimates of ocean primary productivity by remote sensing: The North Atlantic, *J. Geophys. Res.*, **96**, 15,147–15,159, 1991.
- Picaut, J., Propagation of the seasonal upwelling in the eastern equatorial Atlantic, *J. Phys. Oceanogr.*, **13**, 18–37, 1983.
- Rébert, J., J. Donguy, G. Eldin, and K. Wyrski, Relations

- between sea level, thermocline depth, heat content and dynamic height in the tropical Pacific Ocean, *J. Geophys. Res.*, *90*, 11,719-11,725, 1985.
- Reynolds, R. W., and T. M. Smith, Improved global sea surface temperature analyses, *J. Clim.*, *7*, 929-948, 1994.
- Servain, J. A., J. Busalacchi, M. J. McPhaden, A. D. Moura, G. Reverdin, M. Vianna, and S. E. Zebiak, A pilot research moored array in the tropical Atlantic (PIRATA), *Bull. Am. Meteorol. Soc.*, *79*, 2019-2031, 1998.
- Siedler, G., N. Zangenber, R. Onken, and A. Morlière, Seasonal changes in the tropical Atlantic circulation: Observation and simulation of the Guinea Dome, *J. Geophys. Res.*, *97*, 703-715, 1992.
- van Bennekom, A. J., G. W. Berger, W. Helder, and R. T. P. de Vries, Nutrient distribution in the Zaire estuary and river plume, *Netherlands J. Sea Res.*, *12*, 297-323, 1978.
- Voituriez, B., Les sous courants equatoriaux nord et sud et la formation des domes thermiques tropicaux, *Oceanol. Acta*, *4*, 497-506, 1981.
- Williams, R. G., and M. J. Follows, The Ekman transfer of nutrients and maintenance of new production over the North Atlantic, *Deep Sea Res.*, *45*, 461-489, 1998.
- Yamagata, T., and S. Iizuka, Simulation of the tropical thermal domes in the Atlantic: A seasonal cycle, *J. Phys. Oceanogr.*, *25*, 2129-2140, 1995.
- 
- A. J. Busalacchi, C. R. McClain, and R. G. Murtugudde, NASA Goddard Space Flight Center, Laboratory for Hydrospheric Processes, Greenbelt, MD 20771. (e-mail: tonyb@neptune.gsfc.nasa.gov; mcclain@calval.gsfc.nasa.gov; ragu@seetha.gsfc.nasa.gov)
- J. R. Christian, Universities Space Research Association, NASA Goddard Space Flight Center, Greenbelt, MD 20771. (e-mail:jrc@bluefin.gsfc.nasa.gov)
- J. Picaut, L'Institut de Recherche pour le Développement (IRD-ORSTOM), France. (e-mail: jpicaut@neptune.gsfc.nasa.gov)
- S. R. Signorini, NASA Goddard Space Flight Center, Code 970.2, SeaWiFS Project, Building 28, Greenbelt, MD 20771. (e-mail: sergio@bluefin.gsfc.nasa.gov)

(Received December 23, 1998; revised April 12, 1999; accepted April 27, 1999.)